Materials and Methods

Template-Free Synthesis of a Highly Porous Benzimidazole-Linked Polymer for CO_2 Capture and H_2 Storage

Mohammad Gulam Rabbani and Hani M. El-Kaderi*

Department of Chemistry, Virginia Commonwealth University,

1001 W. Main St., Richmond, Virginia 23284

*To whom correspondence should be addressed. E-Mail: helkaderi@vcu.edu

Materials and Methods Table of Contents

Materials and Methods Section S1: *Full synthetic procedures for the preparation of BILP-1.*

General Synthetic Procedures: All starting materials and solvents, unless otherwise noted, were obtained from the Aldrich Chemical Co. and used without further purification. The air sensitive samples and reactions were handled under an inert atmosphere of nitrogen using either glove box or Schlenk line techniques. Tetrakis(4-formylphenyl)methane (TFPM)[1,2,3] and 2,3,6,7,10,11-hexaaminotriphenylene (HATP)[4] were synthesized using published procedures. Elemental microanalyses were performed at the Midwest Microlab, LLC. ^{13}C cross-polarization magic angle spinning (CPMAS) NMR was taken at Spectral Data Services, Inc.

Synthesis of BILP-1: A 100 ml Schlenk flask was charged with 90.0 mg (0.17 mmol) of 2,3,6,7,10,11-hexaamino-triphenylene-hydrochloride salt and 30 ml of anhydrous DMF. The solution was cooled around -30 ºC and a solution of tetrakis(4-formylphenyl)methane (54.0 mg, 0.13 mmol) in anhydrous DMF was added drop-wise. Temperature was maintained around -30 ºC until yellowish brown solid product formation completed and then raised to room temperature and kept for overnight. The flask containing the reaction mixture was flashed with air briefly and capped. The reaction mixture was then heated in an oven at 130 ºC for 3 days to afford a fluffy yellow polymer which was isolated by filtration over a glass frit. The product was immersed in DMF (20 ml) for overnight, and then acetone during which the activation solvent was decanted and freshly replenished twice. The product was drying under vacuum at 120 °C. Anal. Calcd. for $C_{159}H_{84}N_{24}.12H_2O$: C, 74.99; H, 4.27%; N, 13.20%. Found: C, 73.81%; H, 4.97%; N, 12.65%.

Activation of BILP-1 for gas adsorption measurements: A sample BILP-1 was loaded into an autosorb cell and then heated to 120 °C under dynamic vacuum (1.0 x 10^{-5} torr) for 12 h in Masterprap. The sample was finally degassed at 150 °C for 3 h in degassing chamber of autosorb machine prior adsorption measurements. Adsorption measurements were performed on an Autosorb-1 C (Quantachrome) volumetric analyzer.

Supplementary Section S2*: Thermogravimetric Analysis.*

BILP-1 was analyzed by TGA to determine the thermal stability of the material produced as well as confirm that all guests have been removed. Samples were run on a TA Instruments Q-5000IR series thermal gravimetric analyzer with samples held in platinum pans under atmosphere of nitrogen. A 2 ºC/min ramp rate was used.

Figure S1: TGA trace of BILP-1.

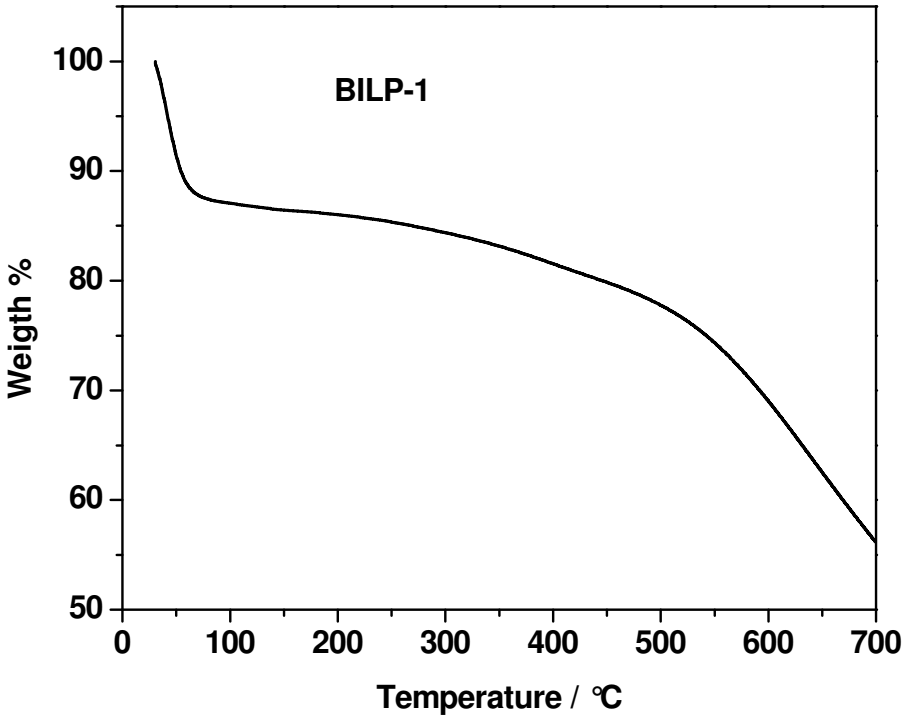

Materials and Methods Section S3: *Scanning Electron Microscopy Imaging (SEM) for BILP-1.*

In order to determine the purity of products, SEM was used to scan for the morphology present in the sample. A sample of the BILP-1 material was subjected to scrutiny under the SEM microscope. Only one type of morphology was found to exist, confirming the purity of the material produced. Sample was prepared by dispersing the material onto a sticky carbon surface attached to a flat aluminum sample holder. The sample was then coated with platinum at $1x10^{-4}$ mbar of pressure in a nitrogen atmosphere for 120 seconds before imaging. Images were taken on a Hitachi SU-70 Scanning Electron Microscope.

Figure S2: SEM image of BILP-1 revealing a spherical morphology.

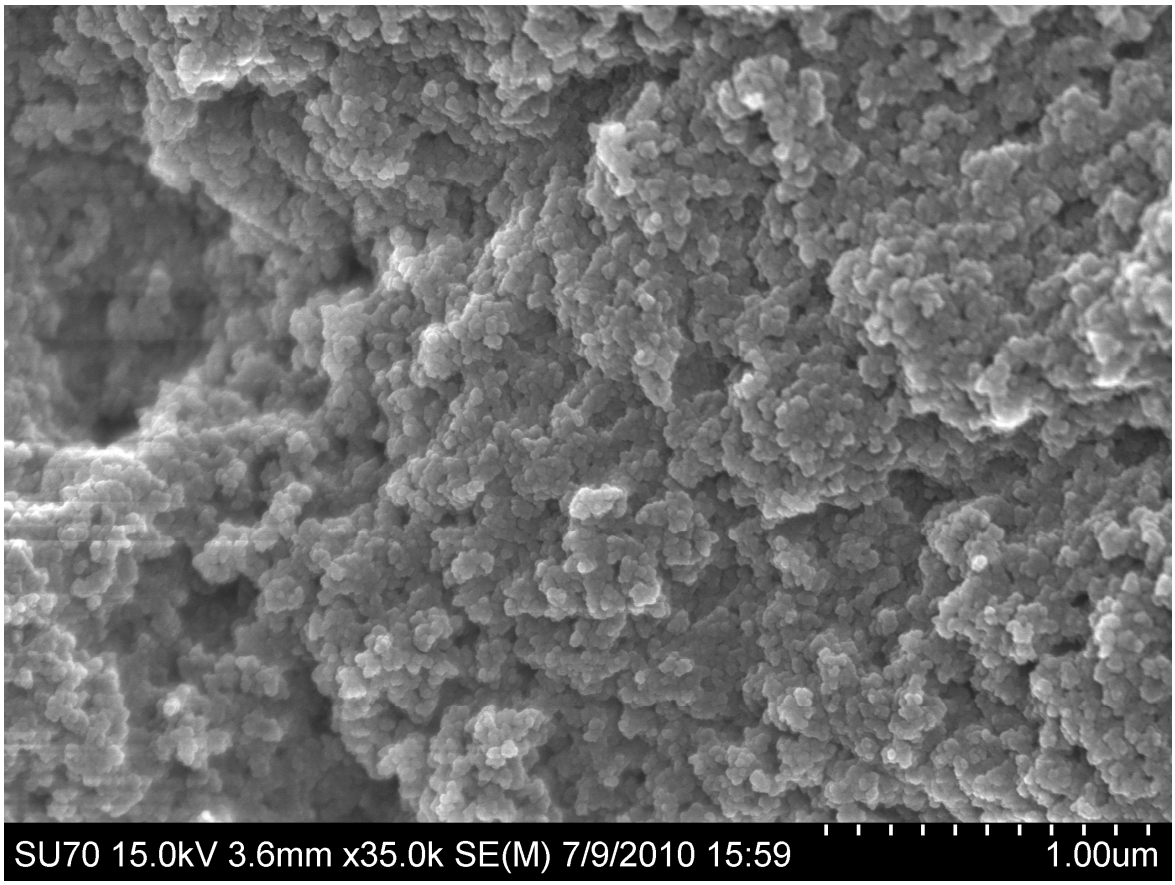

Materials and Methods Section S4: *XRD*-pattern for BILP-1.

Powder X-ray diffraction data were collected on a Panalytical X'pert pro multipurpose difrractometer (MPD). Samples were mounted on a sample holder and measured using Cu Kα radiation with a 2θ range of 1.5-35.

Figure S3: XRD-pattern for BILP-1. Intense peak at 28 is due to the surface characteristics of sample holder. The broad peak at around 2θ=15 indicates the amorphous characteristics of BILP-1.

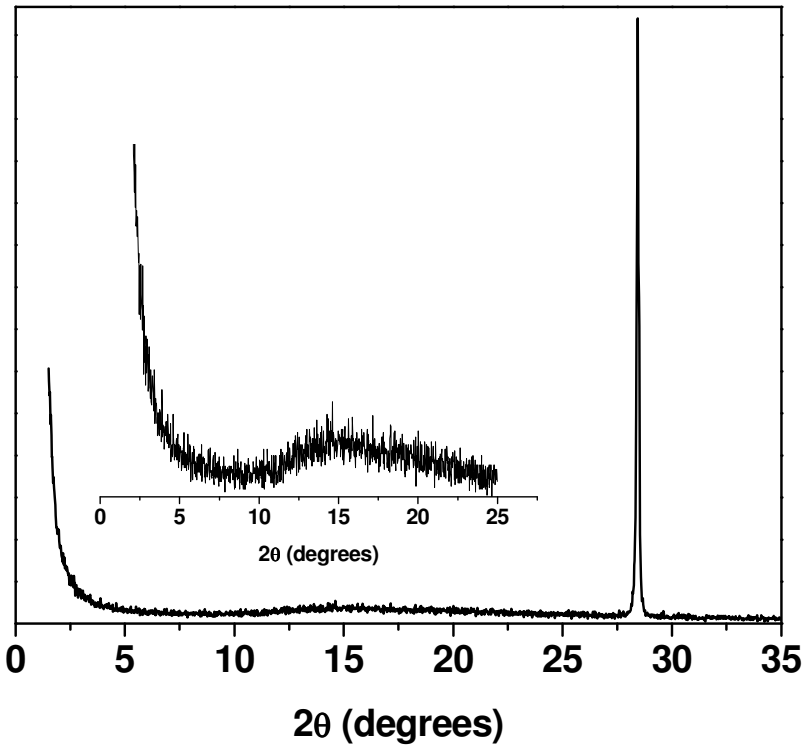

***Materials and Methods Section S5**: FT-IR Spectroscopy of Starting Materials and BILP-1.*

FT-IR spectra of starting materials and synthesized BILP-1 were obtained as KBr pellets using Nicolet - Nexus 670 spectrometer. Assignment and analysis of infrared absorption bands of starting materials and BILP-1 are presented in this section. The data and its discussion pertaining to the IR spectral relationships between these compounds are offered as support for the formation of the covalently linked extended solids.

Figure S4: FT-IR spectra (400-4000 cm^{-1}) of starting materials and BILP-1: The 2736 and 2831 cm^{-1} bands due to C-H stretching of O=C-H in TFPM disappeared in BILP-1. The aromatic C-H stretching was observed around 2800-3100 cm^{-1} in BILP-1. Benzimidazole NH peaks were observed at 3417 (free N-H), 3185 (hydrogen bonded N-H).[5]

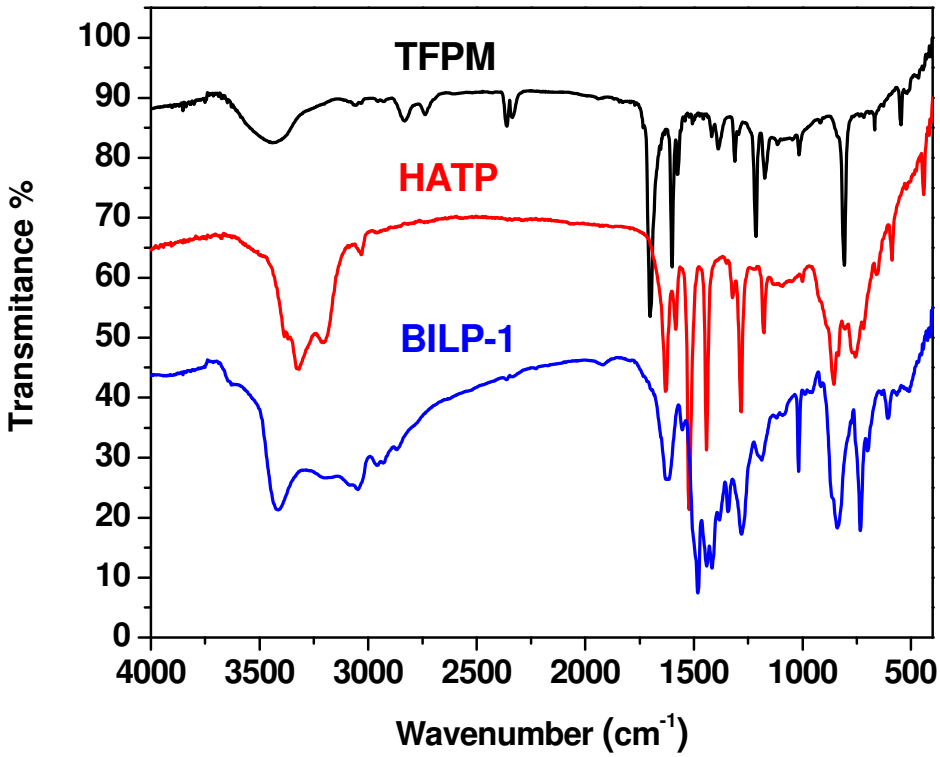

Figure S5: FT-IR spectra (400-1800 cm^{-1}) of starting materials and BILP-1: The intense band at 1702 cm^{-1} due to C=O stretching in TFPM disappeared in BILP-1. There is considerable depletion of the absorption bands for C-N stretching at 1283 cm^{-1} upon benzimidazole ring formation (spectra for HATP and BILP-1). An intense band appeared at 1482 cm^{-1} is assigned to benzimidazole ring.[6] Broad band at around 1625 cm^{-1} presumably due to the mixing of C=C and C=N stretchings.

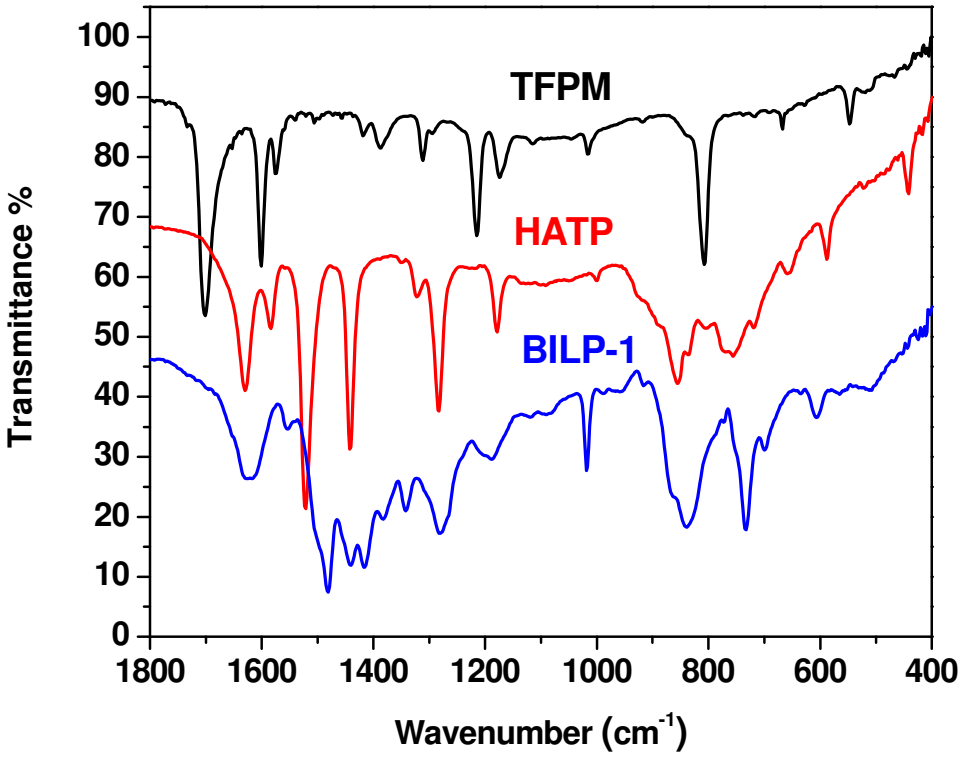

Materials and Methods Section S6*: NMR Studies of Starting Materials and BILP-1.*

Figure S6: ^{13}C NMR spectrum of Tetraphenylmethane (in $CDCl_3$)

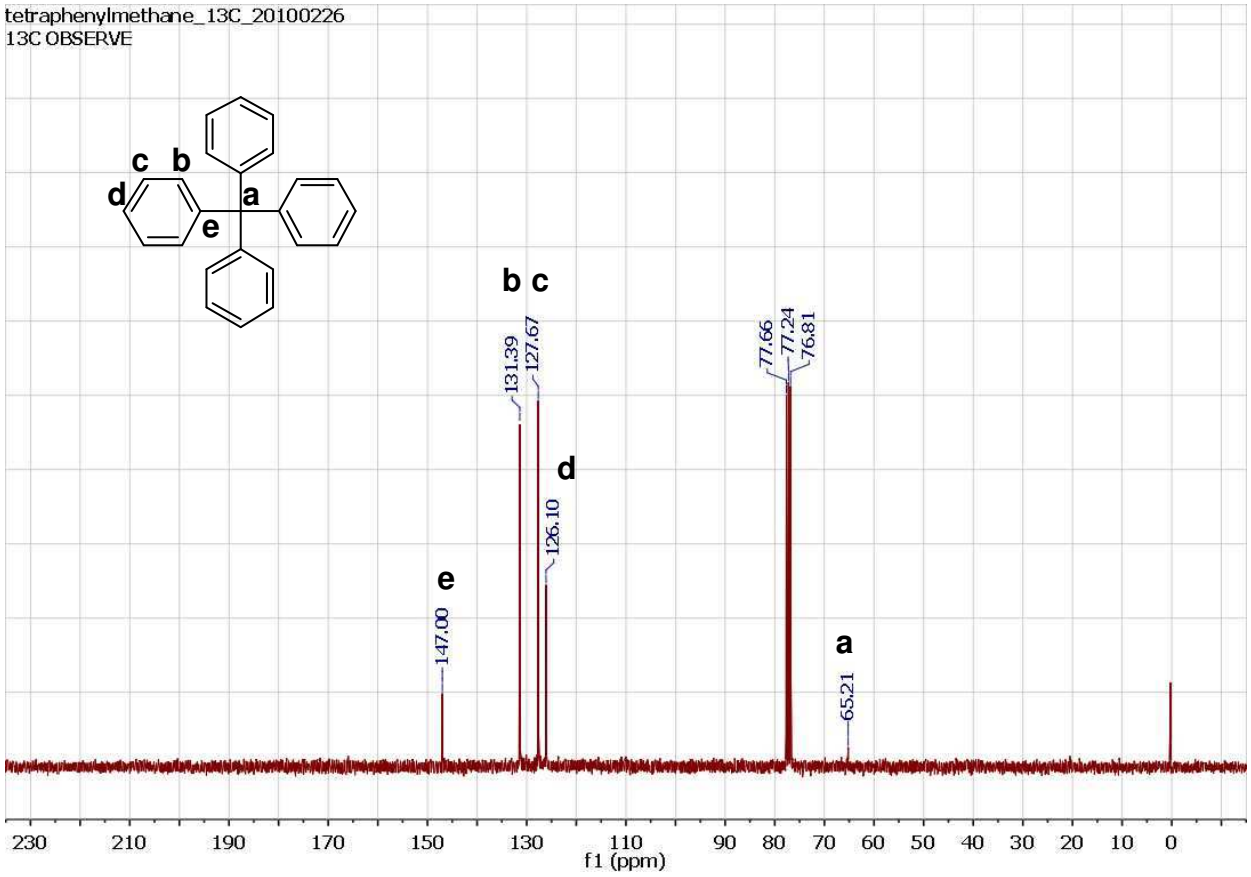

Figure S7: ^{13}C NMR spectrum of TFPM (in $CDCl_3$)

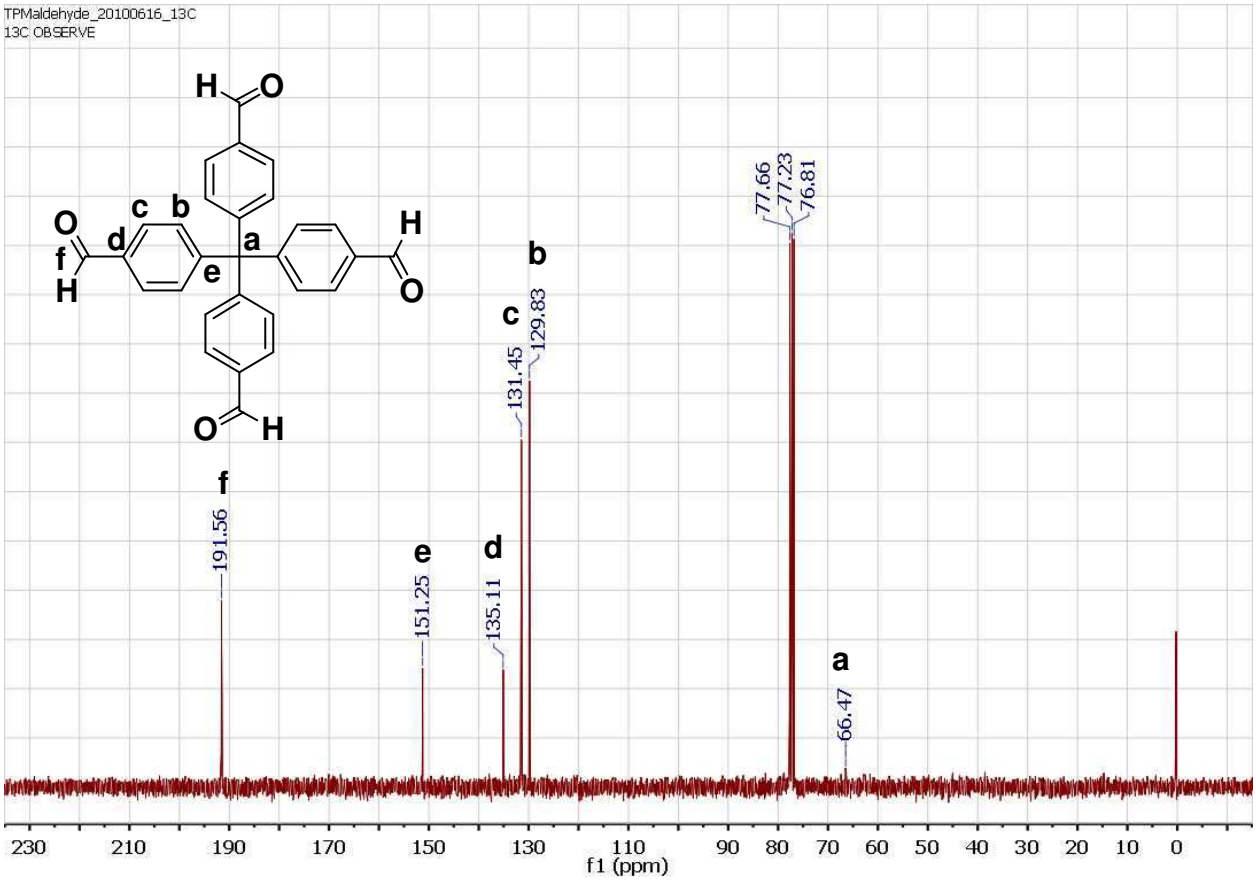

Figure S8: ^{13}C NMR spectrum of HATP (in d_6 DMSO)

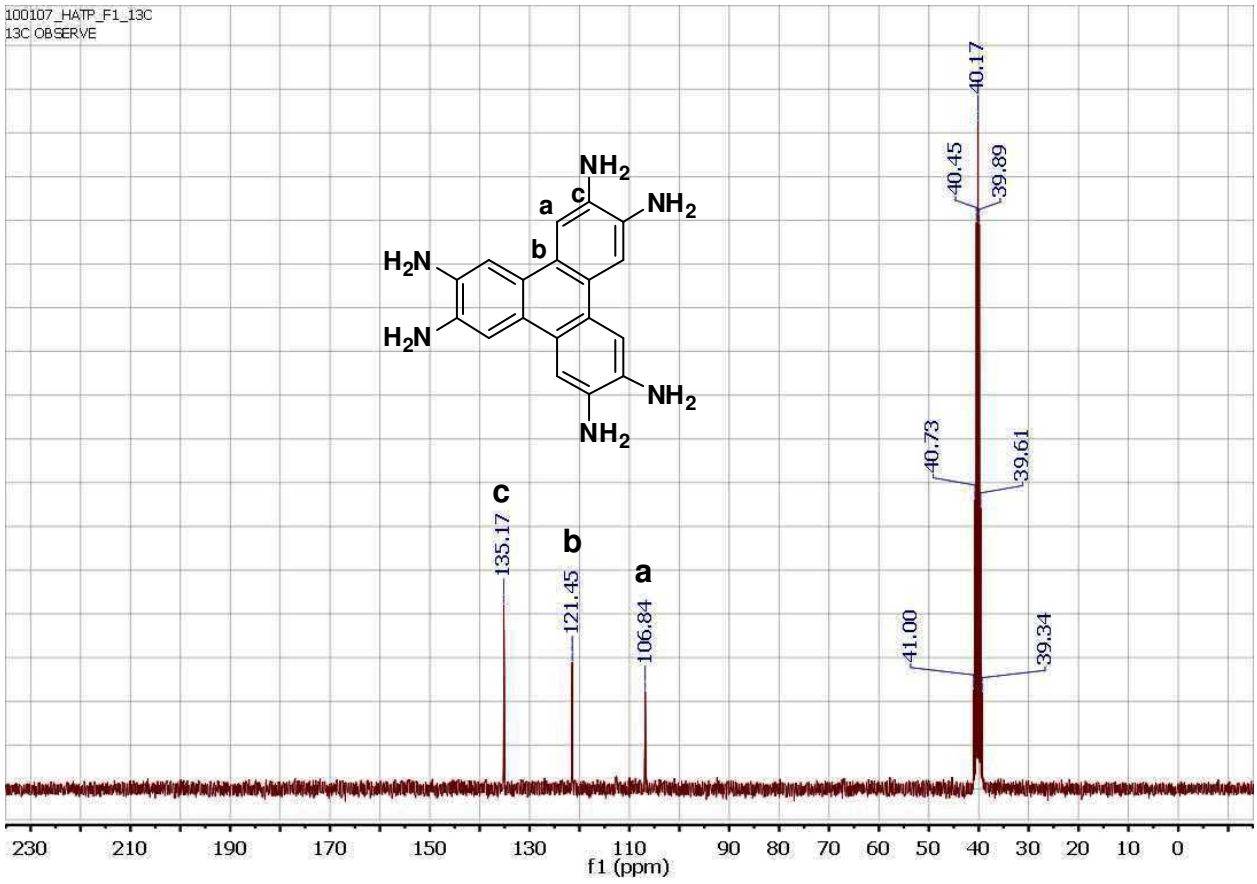

Figure S9: Solid state ^{13}C CP-MAS NMR spectrum of BILP-1.

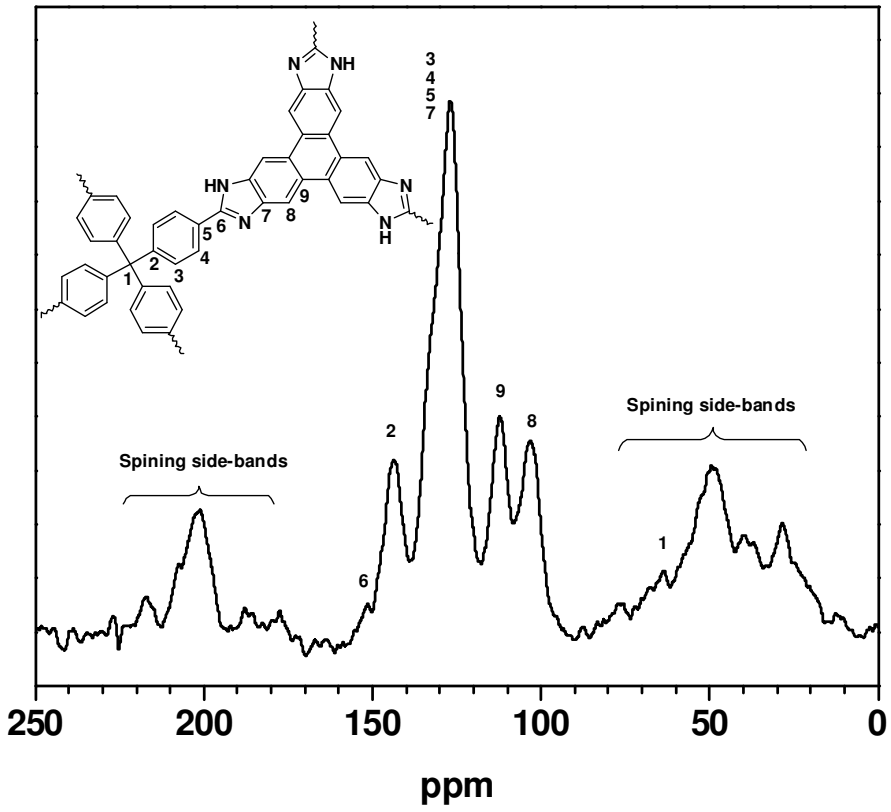

Assignments of the ^{13}C CP-MAS NMR peaks.

Peaks (ppm)	Assignments
65	Quaternary C1. This quaternary carbon usually gives weak peak and this is overlapped here by spinning side-bands.
104	Triphenylene C8. This is observed at 107 ppm in HATP (d_6-DMSO).
112	Triphenylene C9. This is observed at 121 ppm in HATP (d_6-DMSO).
127-135	Aromatic carbon C3, C4, C5, C7. The peaks due to C3, C4 and C5 are observed at 130, 131 and 135 ppm, respectively, in TFPM ($CDCl_3$). The peak due to triphenylene C7 is observed at 135 ppm in HATP (DMSO-d_6).
144 (with a shoulder peak at151)	Aromatic C2. This is observed at 147 and 151 ppm in tertraphenylmethane and TFPM, respectively ($CDCl_3$). The shoulder peak at 151 ppm is due to benzimidazole C6. It is noted that no peak was observed around 160 ppm for imine C=N. This suggests the successful formation of benzimidazole ring.

Supplementary Section S7: Low Pressure (0 – 760 mmHg) Gas Adsorption Measurements for BILP-1.

Figure S10: N_2 adsorption isotherm for BILP-1 measured at 77 K. The filled circles are adsorption points and the empty circles are desorption points.

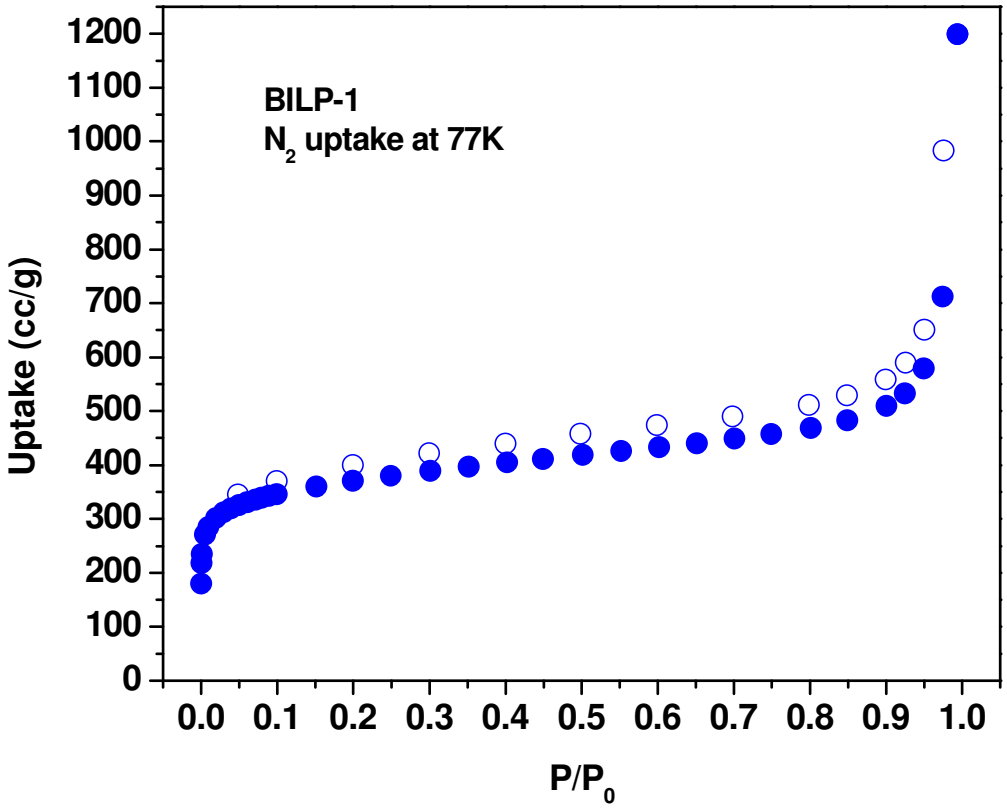

Figure S11: Experimental N_2 adsorption isotherm for BILP-1 measured at 77 K is shown as filled circle. The calculated NLDFT isotherm is overlaid as open circle. Note that a fitting error of < 1 % indicates the validity of using this method for assessing the porosity of BILP-1. The fitting error is indicated.

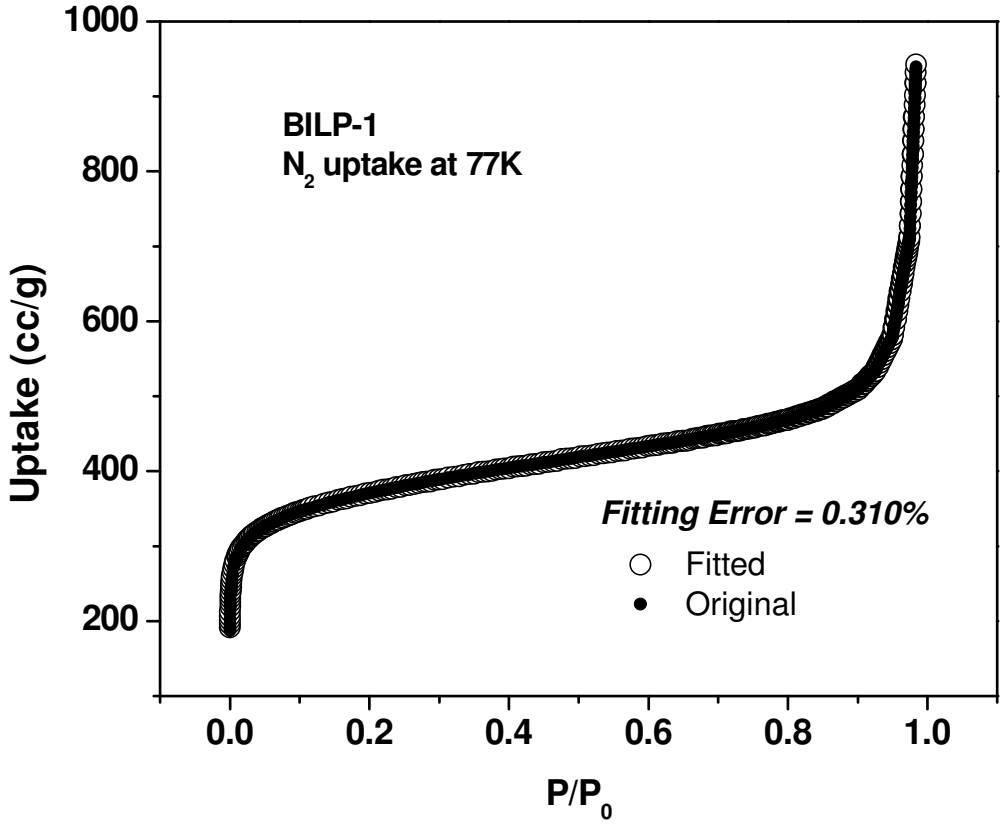

Figure S12: BET plot for BILP-1 calculated from the N_2 adsorption isotherm at 77 K. The model was applied from P/P_o= 0.05-0.15. The correlation factor is indicated. (W = Weight of gas absorbed at a relative pressure P/P_o).

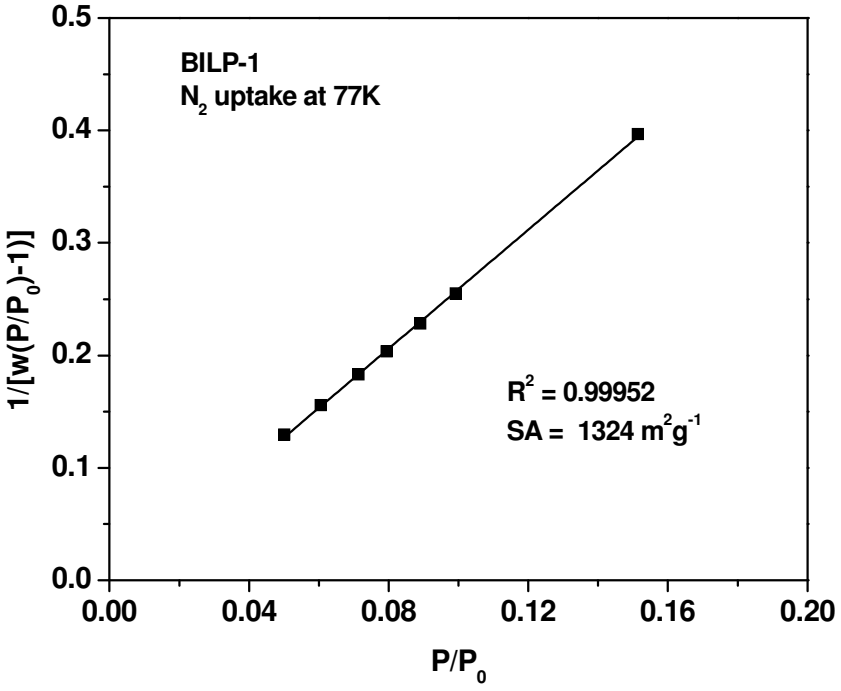

Figure S13: Ar adsorption isotherm for BILP-1 measured at 87 K. The filled circles are adsorption points and the empty circles are desorption points

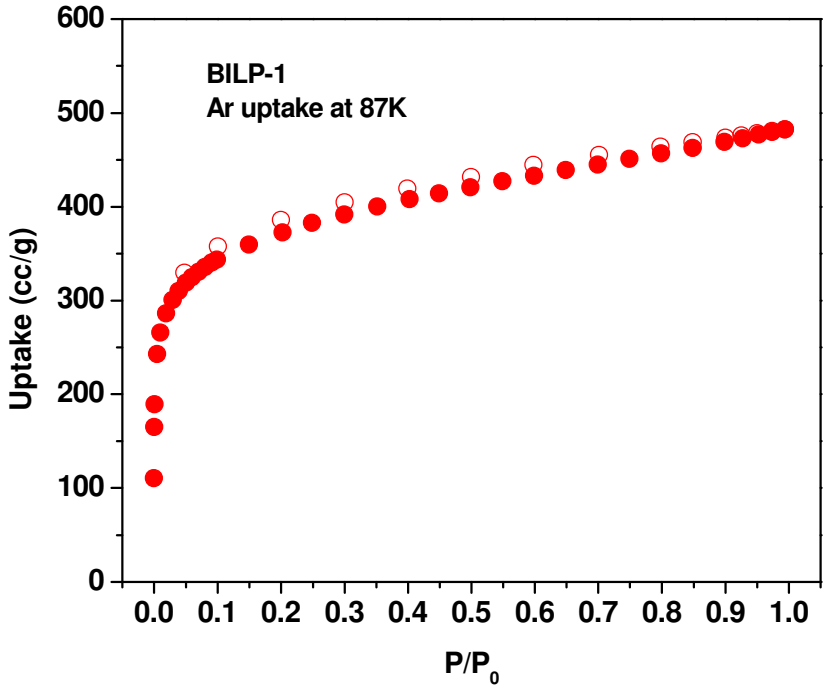

Figure S14: The Pore Size Distribution of BILP-1 was calculated from the Ar adsorption isotherm by the Non-Local Density Functional Theory (NLDFT) method using a cylindrical pore model.

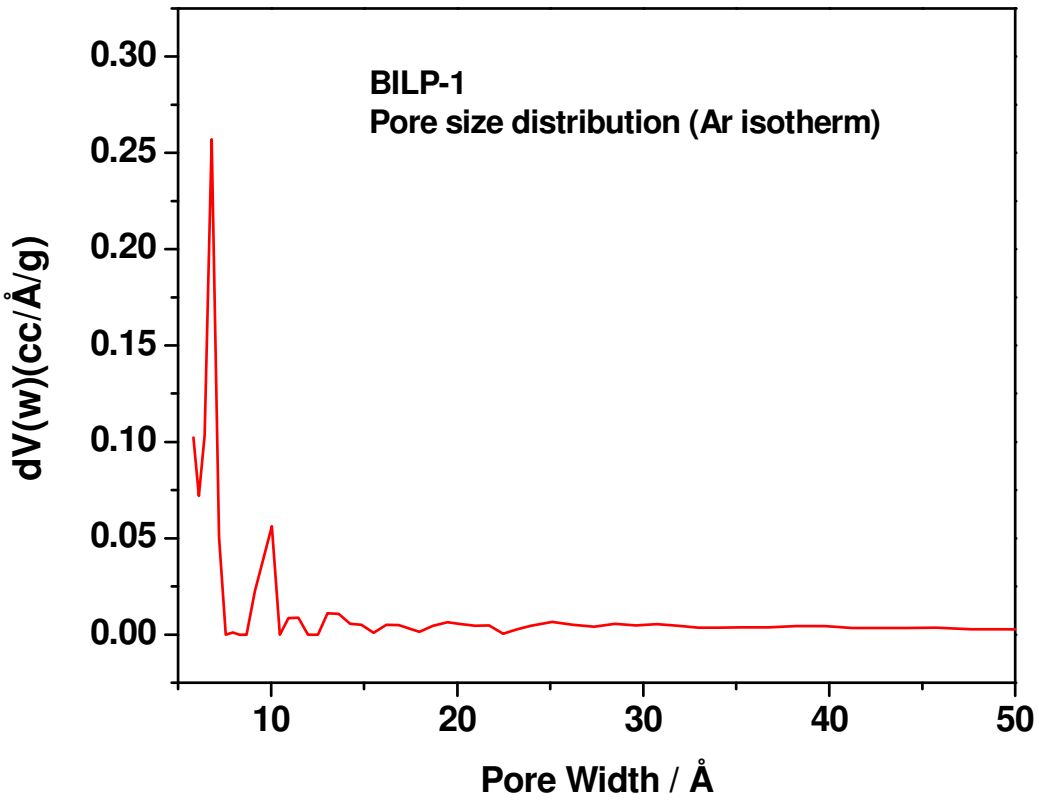

Pore Width (Mode) = 6.8 Å

Pore Volume = 0.6977 cc/g

Figure S15: Experimental Ar adsorption isotherm for BILP-1 measured at 87 K is shown as filled circle. The calculated NLDFT isotherm is overlaid as open circle. Note that a fitting error of < 1 % indicates the validity of using this method for assessing the porosity of BILP-1. The fitting error is indicated.

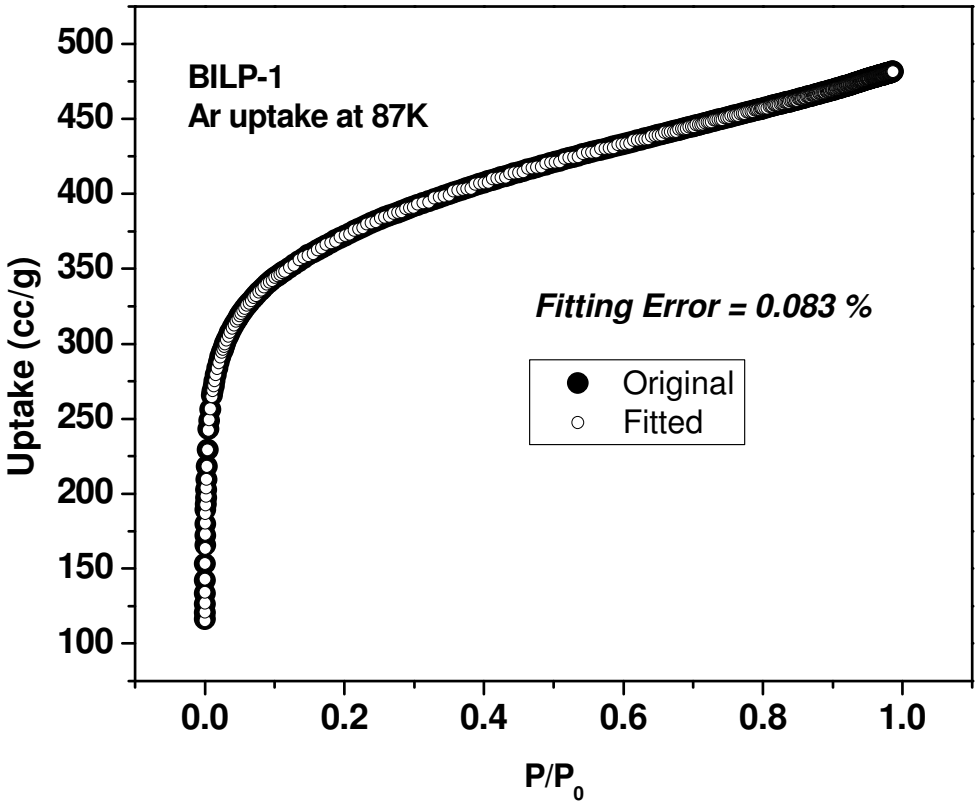

Figure S16: BET plot for BILP-1 calculated from the Ar adsorption isotherm at 87 K. The model was applied from P/P_o= 0.05-0.15. The correlation factor is indicated. (W = Weight of gas absorbed at a relative pressure P/P_o).

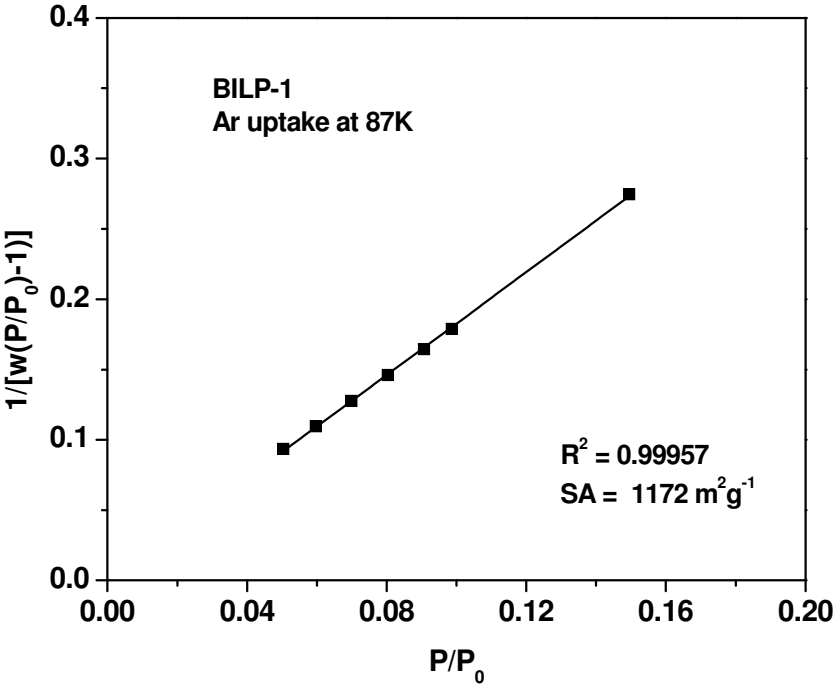

Figure S17: Virial analysis of CO_2 adsorption data (A) (circles: 298 K, squares: 273 K) and isosteric heat of adsorption (Q_{st}) (B) for BILP-1. a0 = -3207.28789737649, a1= 255.869741564136, a2 = -24.6931049390554, a3 = 2.51137210962288, b0 = 15.1568962989967, b1 = -0.302172298468563

.

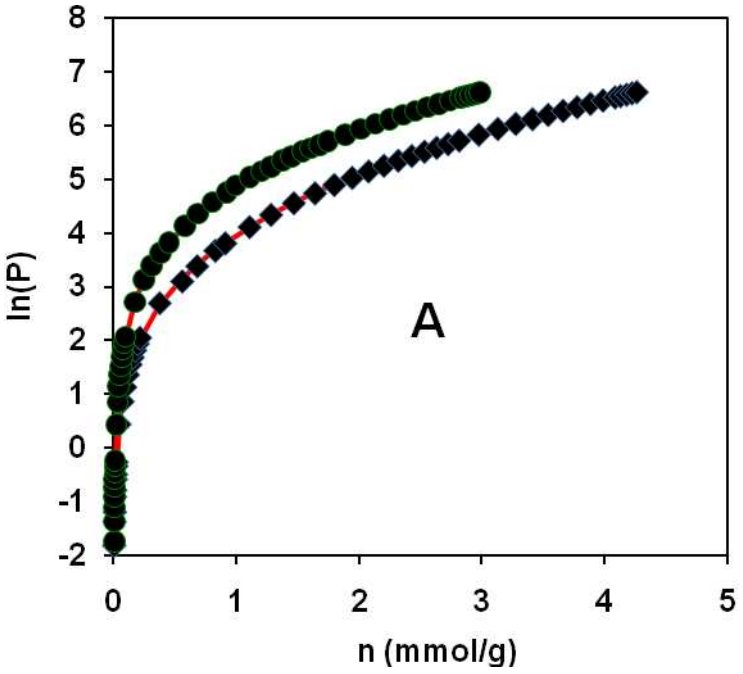

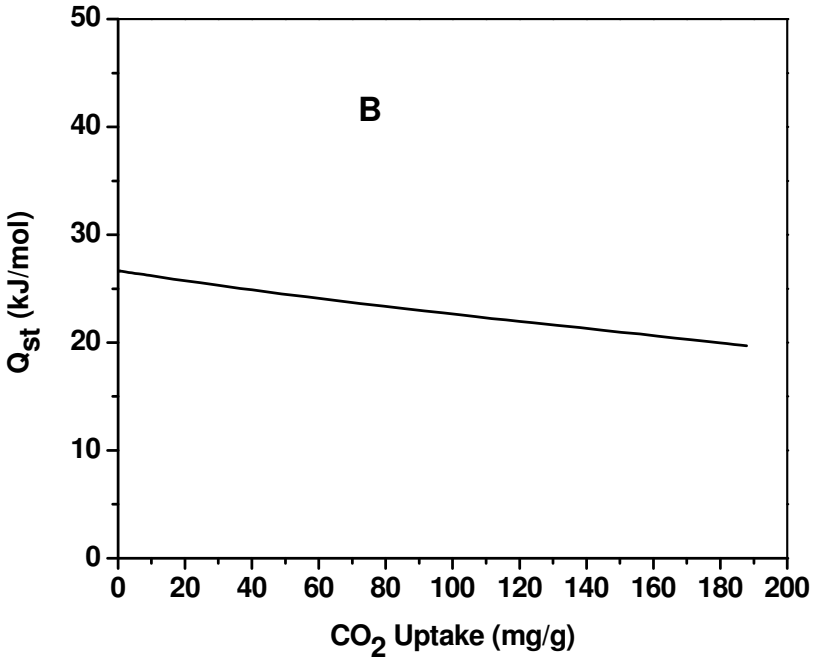

Figure S18: Virial analysis of H_2 adsorption data (A) (circles: 87 K, squares: 77 K) and isosteric heat of adsorption (Q_{st}) (B) for BILP-1. a0 = -958.408247318236, a1= 33.1278324303581, a2 = -0.583863085674663, b0 = 13.3860113709155.

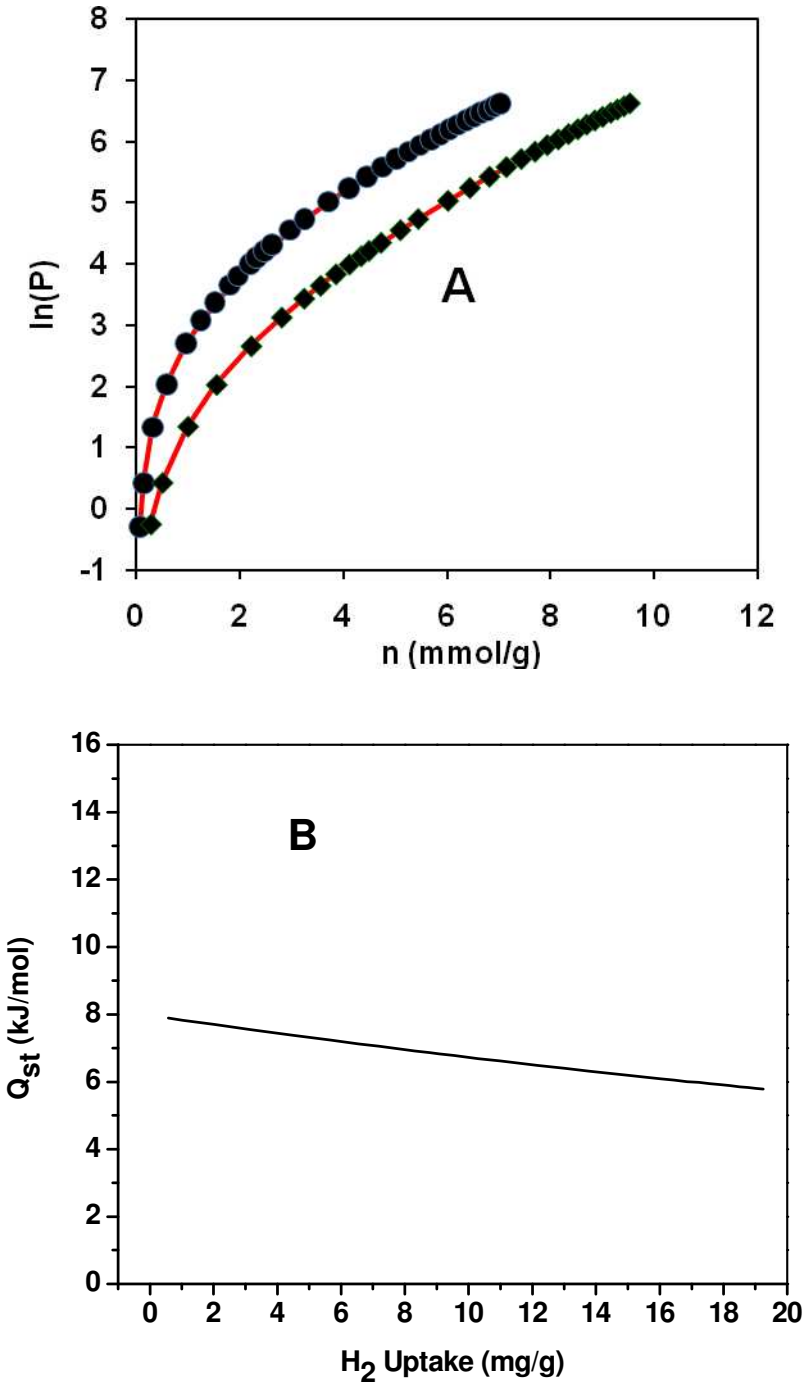

Figure S19: Virial analysis of CH_4 adsorption data (A) (circles: 298 K, squares: 273 K) and isosteric heat of adsorption (Q_{st}) (B) for BILP-1. a0 = -1959.37490232843, a1= 277.504790020752, a2 = 629.380033105775, a3 = - 525.039553883211, a4 = 147.369870108566, b0 = 13.0521227667298, b1 = -1.66551627519581

.

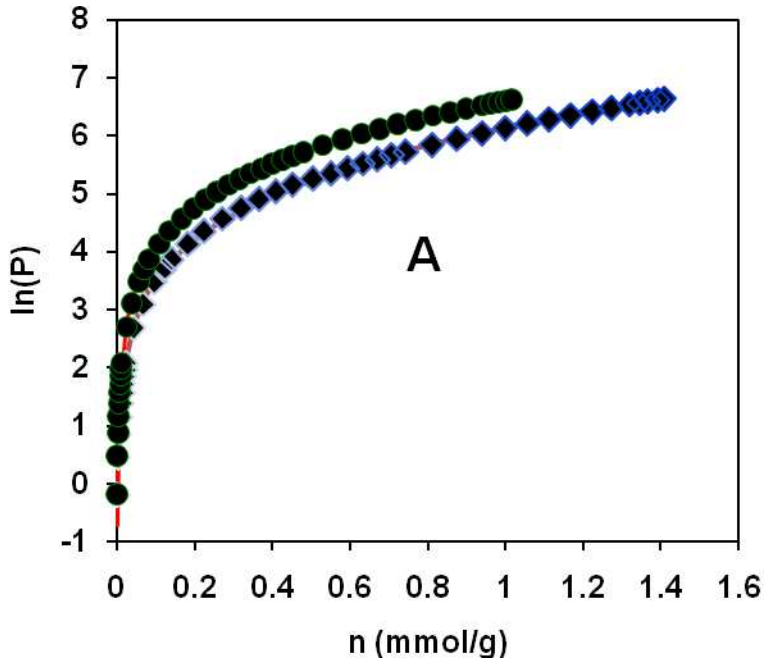

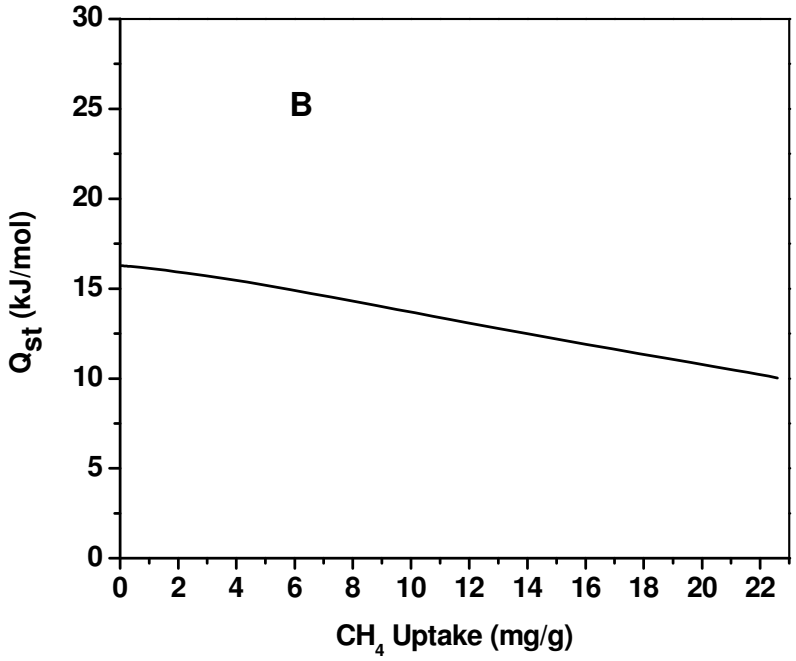

Figure S20: Adsorption isotherms for BILP-1 at 273 K (A) and 298 K (B); CO_2 (black), CH_4 (blue) and N_2 (red). The filled shapes are adsorption points and the empty shapes are desorption points.

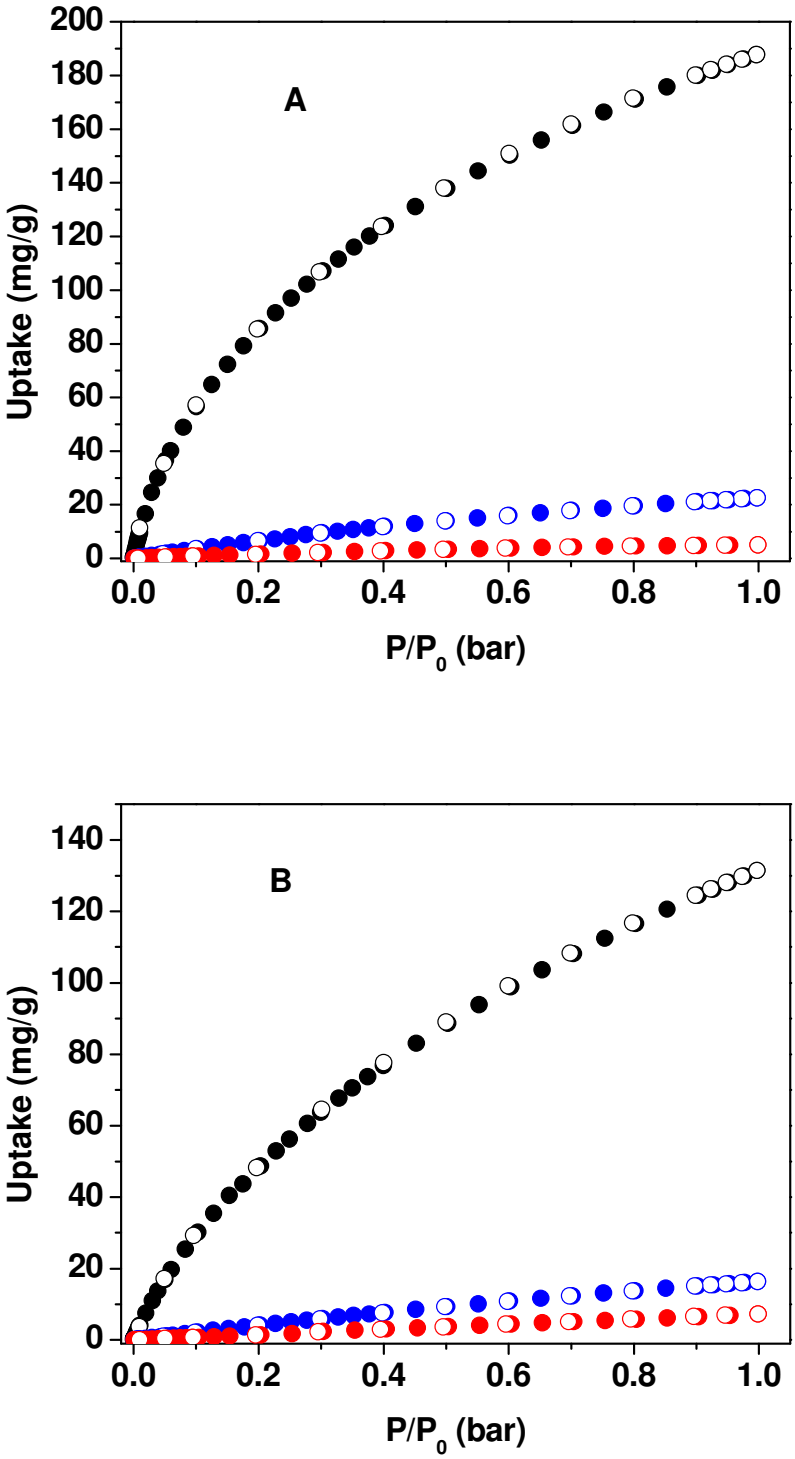

Figure S21: Adsorption selectivity of CO_2 over N_2 and CH_4 for BILP-1 from initial slope calculations. CO_2 (black), CH_4 (red) and N_2 (blue) isotherms collected at 273 K (A) and 298 K (B).

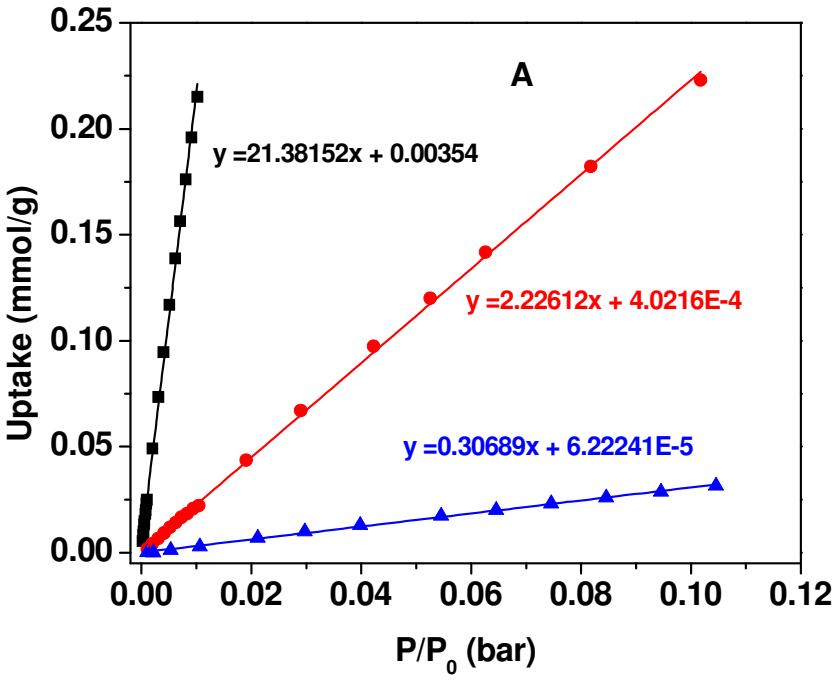

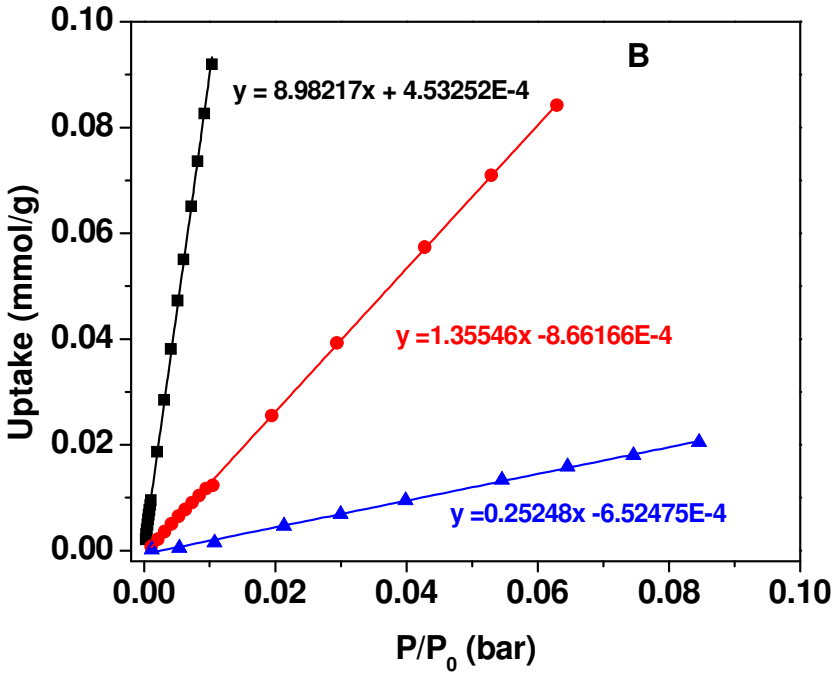

References

1. Ganesan, P.; Yang, X.; Loos, J.; Savenije, T. J.; Abellon, R. D.; Zuilhof, H.; Sudhölter, E. J. R., *J. Am. Chem. Soc*., **2005**, *127*, 14530.

2. Rathore, R.; Burns, C. L.; Guzei, I. A., *J. Org. Chem*. **2004**, *69*, 1524–1530.

3. Fournier, J.-H.; Wang, X.; Wuest, J. D., *Can. J. Chem*. **2003**, *81*, 376-380.

4. Chen, L.; Kim, J.; Ishizuka, T.; Honsho, Y.; Saeki, A.; Seki, S.; Ihee, H.; Jiang, D., *J. Am. Chem. Soc.*, **2009**, *131*, 7287–7292.

5. (a) Bouchet, R.; Siebert, E., Solid State Ionics,1999, 118,287–299 (b) Feng, S.; Shang, Y.; Wang,S.; Xie, X.; Wang, Y.; Wang, Y.; Xu, J., *J. Membr. Sci*., **2010**, *346*, 105–112.

6. (a) Schoone, K.; Smets, J.; Houben, L.; Bael, M. K. V.; Adamowicz, L.; Maes, G., *J. Phys. Chem. A* **1998**, *102*, 4863-4877. (b) Morsy, M. A. ; Al-Khaldi, M. A.; Suwaiyan, A., *J. Phys. Chem. A* **2002**, *106*, 9196-9203 (c) Sundaraganesan, N.; Ilakiamani ,S.; Subramani , P.; Joshua, B. D., *Spectrochim. Acta A* **2007**, *67*, 628–635.